machines

MDPI

Article

Design Guidelines for Fractional Order Cascade Control in DC Motors: A Computational Analysis on Pairing Speed and Current Loop Orders Using Oustaloup's Recursive Method

Marta Haro-Larrode * and Alvaro Gomez-Jarreta

Department of Electrical Engineering, School of Engineering and Architecture, University of Zaragoza, Maria de Luna 3, 50018 Zaragoza, Spain; 758639@unizar.es

* Correspondence: mharolarrode@unizar.es

Abstract: Nested, or cascade speed and torque control has been widely used for DC motors over recent decades. Simultaneously, fractional-order control schemes have emerged, offering additional degrees of control. However, adopting fractional-order controllers, particularly in cascade schemes, does not inherently guarantee better performance. Poorly paired fractional exponents for inner and outer PI controllers can worsen the DC motor's behavior and controllability. Finding appropriate combinations of fractional exponents is therefore crucial to minimize experimental costs and achieve better dynamic response compared to integer-order cascade control. Additionally, mitigating adverse couplings between speed and current loops remains an underexplored area in fractional-order control design. This paper develops a computational model for fractional-order cascade control of DC motor speed (external) and current (internal) loops to derive appropriate combinations of internal and external fractional orders. Key metrics such as overshoot, rise time, and peak current values during speed and torque changes are analyzed, along with coupled variables like speed drop during torque steps and peak torque during speed steps. The proposed maps guide the selection of effective combinations, enabling readers to deduce robust or adaptive designs depending on specific performance needs. The methodology employs Oustaloup's recursive approximation to model fractional-order elements, with MATLAB–SIMULINK simulations validating the proposed criteria.

Keywords: fractional-order control; DC motor; speed and torque control; cascade control; Oustaloup recursive method

Academic Editors: Parviz Famouri and Payam Shams Ghahfarokhi

Received: 10 December 2024
Revised: 6 January 2025
Accepted: 14 January 2025
Published: 16 January 2025

Citation: Haro-Larrode, M.; Gomez-Jarreta, A. Design Guidelines for Fractional Order Cascade Control in DC Motors: A Computational Analysis on Pairing Speed and Current Loop Orders Using Oustaloup's Recursive Method. *Machines* **2025**, *13*, 61. https://doi.org/10.3390/machines13010061

1. Introduction

In the last decade, there have been many advances in the development of fractional-order control schemes (FOCSs) [1–4], and the benefits of implementing an extra control freedom degree provided by the use of fractional orders over pure integer order control schemes (IOCSs) [5–8] for DC motors have been highlighted. However, if not adequately selected, the fractional orders may also contribute to oscillatory behavior in DC motors, as reported in [8,9]. Many studies have been oriented at demonstrating the superiority of fractional- over integer-order control, but very few [8,9] explore the adverse effects. For this purpose, the employment of continuous approximations for representing a fractional-order term is a valid mathematical tool to analyze in a much easier way the performance of a system, as demonstrated in previous studies [10–12].

Fractional calculus has been applied in plenty of fields, such as the positioning of servo systems [5,13], fluid mechanics [7,14], the control of electronic converters [8,9], en-

ergy applications [15,16], materials [17], and unmanned aerial vehicles (UAVs) [18]. The latter field has increased its relevance within the last decade, as UAVs present inspection and delivery capabilities in many industrial and civilian applications, such as powerline inspection [19–22], forest fire detection [23,24], and the delivery of goods [25], among others [26–29]. The key elements of a quadrotor UAV are the DC motors, which are responsible for the global thrust that makes the UAV hover, and the different trajectories that the UAV can follow, thanks to combined control commands sent to the DC motors in pairs.

To achieve the optimal performance of electric motors, it is essential to develop highly efficient control schemes, as they play a crucial role in enhancing motor performance. Therefore, recent work regarding the fractional order (FO) control of different electric motors and other devices has been summarized, with a special focus on those FO control schemes tuned with optimization algorithms. In [30], a novel sensorless direct torque control design was developed for a five-phase induction motor with an intelligent estimator based on an FO controller. In this case, the FO controller parameters are obtained via a particle swarm optimization algorithm to enhance the reference model adaptive system. With this novel method, the dynamic stability is enhanced, the rotor speed overshoot is canceled, the response time is improved, and the torque ripple is minimized compared to other methods. The authors claimed that this combination is more robust and suitable for five-phase motor applications and planned experimental test benches to further improve sensorless control in multiphase motors. As for speed sensing, incremental encoders, although they are very often used for measuring the speed in motor drives, can introduce issues in the measurement of motor speed that may affect the control system performance, especially at low speeds. Incremental encoders have imposed practical limitations due to the limited resolution for low speeds, noise in the speed signal due to mechanical vibrations, and measurement delays. Therefore, these issues may require changes in the selected gains when implementing the control schemes these devices into experimental practice [31]. In [12], the authors implemented a low-order approximation method for the FO PID controller based on the improved artificial bee colony algorithm, which turned out to outperform PID controllers optimized by other algorithms in terms of transient response, robustness testing, and disturbance rejection in an automatic voltage regulator (AVR) system. In [32], a review of integer- and fractional-order PID controllers using optimization techniques for speed control for a brushless DC motor drive was accomplished. The article concludes that the FO PID controllers optimized with techniques such as the bat algorithm demonstrate superior performance compared to other controllers and optimization methods.

Many studies exist regarding the modeling and control of a DC motor, as reported in [32–34]. However, little attention has been given to the possibility of implementing a fractional-order control scheme for the DC motor, and only a few studies [32,35] have considered this. Furthermore, since it is one of the most established cascade control schemes in the control engineering field, very few authors have considered FOCS [1,10,13], and to the best knowledge of the authors of this study, none of these researchers have studied the combined impact of the FO exponents of current (internal) and speed (external) PIs within a cascaded structure. In nested control systems, collateral effects often arise from the dynamic interaction between nested control loops, and when implemented within a fractional-order control structure, this aspect deserves attention, as an additional control degree may be used to improve the behavior of DC motors, but it also may lead to a worsening if the fractional orders of the current and speed loops are not suitably paired. This research dispels the idea that controllers with an additional degree of freedom automatically outperform others.

In this paper, a computational analysis is developed for FOCS-based DC motor models to obtain pairing criteria for fractional-order PI exponents of both the current and speed loops of the DC motor under small torque and speed steps. For this purpose, in Section 2, the well-established Oustaloup recursive method is chosen as the implementation method to build the FOCS-based DC motor models, as well as the description of the cascade control scheme with fractional-order PIs. In Section 3, the methodology followed by this paper is described. In Section 4, a preliminary integer-order control simulation study is carried out on the DC motor to set the proportional and integral control parameters of the inner and outer PI controllers of the DC motor, which will not be varied during the subsequent comparative analyses, and that ensure good DC motor behavior while, in turn, allowing room for improvement. In Section 5, simulations are carried out for different FOCS-based DC motor models corresponding to different fractional orders in comparison to the IOCS-based DC motor model, by demonstrating that the differential pairing of the fractional orders of speed and current PI controllers may lead to improvements in, or preservations or deteriorations of the different metrics observed in the DC motor's behavior, i.e., overshoot, rise time, peak current, and torque and speed drops. To understand how the pairing of fractional orders of speed and current PI controllers affects the different metrics, in Section 6, an impact analysis is carried out for different fractional orders of the speed and current PI controllers, and, consequently, pairing criteria are derived to improve each metric separately with respect to those from the IOCS-based DC motor. The occurrence of a torque peak in response to a speed step and a transient speed decrease in response to a torque step indicate coupling between the current and speed control loops within the cascade scheme. The combined influence of the internal current loop and external speed loop is also analyzed, and metrics considering the coupling between inner and outer loops are also included in the analysis when pairing current and speed fractional-order PI exponents. Once the influence of each fractional order pairing is clarified, 3D plots are built to summarize the criteria for each metric, which represent an improvement over the IOCS-controlled DC motor. Once the previous analyses are conducted in a separate way for each metric, maps are built to allow the reader to derive either a robust or an adaptive control design for the DC motor control system, to improve simultaneously or separately different metrics compared with the results observed in the IOCS-based DC motor. In Section 7, a discussion is established regarding the impact of considering more profound speed and torque changes, and how these impact the different metrics, to allow the reader to refine the pairing of fractional orders according to different specifications. In Section 8, the main conclusions are drawn. The main implication of this study is the use of computational analysis to save costs in a future experimental study.

The main contributions of this paper are summarized below:

1. The selection of an appropriate approximation degree for fractional-order terms: the application of Oustaloup's recursive method to select the appropriate approximation degree for fractional-order terms in the speed and current control loops of a cascade control system for DC motors.
2. Impact analysis on key metrics: A computational analysis to assess the influence of speed (λ_e) and current (λ_i) fractional orders on rise time and overshoot levels under generic speed and torque step changes. The analysis is performed on a comparative basis, taking the IOCS-controlled DC motor as a reference and by having the same proportional and integral constants in both the IOCS- and FOCS-controlled DC motor models. In this way, the effect of fractional-order pairings is clarified over those of other control parameters.

3. Dynamic coupling assessment: A computational analysis to assess the influence of speed (λ_e) and current (λ_i) fractional orders on coupled loop dynamics, including transient torque peaks during a speed change and transient speed drops during a torque change. The analysis is made on a comparative basis, taking the IOCS-controlled DC motor as a reference and by having the same proportional and integral constants in both the IOCS-and FOCS-controlled DC motor models. In this way, the effect of fractional-order pairings is clarified over those of other control parameters.
4. Optimal pairing criteria: the determination of pairing criteria for speed (λ_e) and current (λ_i) fractional orders that improve key and coupled metrics in comparison to those observed in the IOCS-controlled DC motor model, providing insights on robust and adaptive design guidelines.
5. Extension to other torque and speed changes: the expansion of pairing criteria for speed (λ_e) and current (λ_i) fractional orders to address more profound torque and speed variations.

The proposed analysis excludes DC motor startups and shutdowns, as the focus is on torque and speed step responses.

2. Problem Formulation

In this section, the main theoretical formulation that defines the problem to be addressed is presented. For this purpose, first, a background on fractional-order theory and the employed approximation method is given in Section 2.1. In Section 2.2, the implementation of FO PI controllers in the cascade control scheme and the main DC motor equations are described.

2.1. Employed Approximation Method for Representing the Fractional-Order Term

The rational approximation for the $s^{-\lambda}$ term consists in integer-order polynomial terms and, thus, it is possible to work, since it is an integer-order system, as was demonstrated in [8], with proportional resonant controllers. In [2,3,8], Continuous Fraction Expansion (CFE), Carlson, Oustaloup, and Matsuda approximation methods were employed to represent the non-rational $s^{-\lambda}$ term. Regardless of the employed approximation method, the stable area for a fractional-order integrator with $0 < |\lambda| < 1$ is enlarged with respect to that for an integer-order integrator [12], as shown in Figure 1.

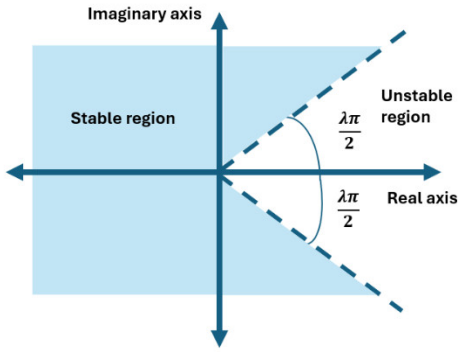

Figure 1. Stable and unstable regions when $0 < \lambda < 1$.

In Table 1, the stability limits are shown for every λ value. So, as far as the absolute value of λ is reduced, the unstable region is smaller, whereas for λ closer to 0.9, the unstable region is wider.

Table 1. Stability limits for fractional-order integrators.

$\lvert\lambda\rvert$	**Phase =** $\lvert\lambda\rvert$ **90 (°)**
0.1	9
0.2	18
0.3	27
0.4	36
0.5	45
0.6	54
0.7	63
0.8	72
0.9	81
1	90

However, to accurately represent phenomena within certain frequency ranges, it is necessary either to increase the degree of the approximation method functions or to employ more advanced methods, such as the Oustaloup recursive method, which is the most frequently used continuous approximation method [36]. The generalized Oustaloup's recursive method for a fractional derivative of order λ is defined in (1)–(4), for a frequency range of $[\omega_b, \omega_h]$, where the N-degree polynomial approximation is valid and where $\omega\prime_k$ and ω_k are obtained through recursive equations:

$$s^{\lambda} \cong \omega_h^{\lambda} \prod_{k=1}^{N} \frac{s + \omega\prime_k}{s + \omega_k} \tag{1}$$

$$\omega\prime_k = \omega_b \mu^{\frac{2k-1-\lambda}{N}} \tag{2}$$

$$\omega_k = \omega_b \mu^{\frac{2k-1+\lambda}{N}} \tag{3}$$

$$\mu = \sqrt{\omega_h / \omega_b} \tag{4}$$

In Figure 2, the different degrees of approximation, N = 2, 4, 6, and 8, in Oustaloup's recursive method are used to model different fractional integrators, $s^{-\lambda}$, namely with λ = 0.2, 0.4, 0.6, and 0.8. As the approximation degree increases, the phase bode plots tend to have less oscillations, and the greater the order, the better the accuracy. The oscillations are wider for lower fractional exponents, such as λ = 0.2 or 0.4, whereas for higher fractional exponents, the oscillations are lower. In any case, the plots in Figure 2 suggest that for modeling any fractional-order integrator from λ = 0.1 to λ = 0.9, a high order must be chosen to cover all the λ values. By looking at the approximation degree, N = 8 is a sufficiently good order to be valid in the range of frequency until 10^6 rad/s. This defines a time window accuracy of 6.28 μs, which is enough accuracy for the corresponding simulation study, as it will be recalled in the corresponding section. Therefore, the approximation degree with N = 8 with Oustaloup's recursive method will be used to represent the complete set of fractional orders.

Once the approximation method and degree for the $s^{-\lambda}$ term have been chosen, the transfer function for fractional-order PIs can be computed. A freely downloadable software package called FOMCON (version v1.50.4) [37] will be used for the next impact analyses.

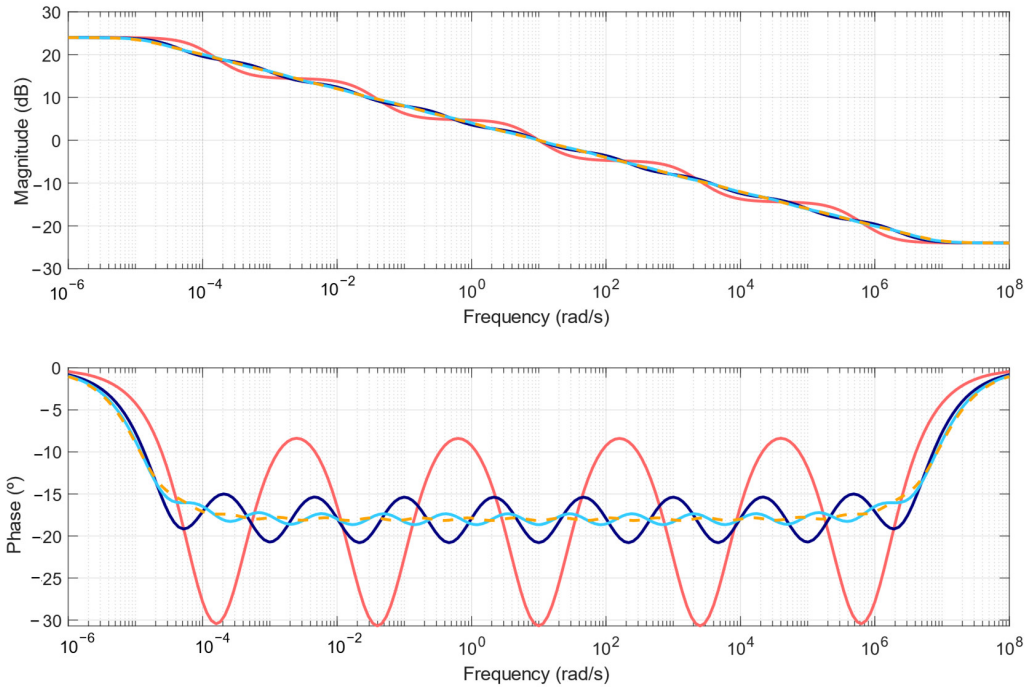

(a)

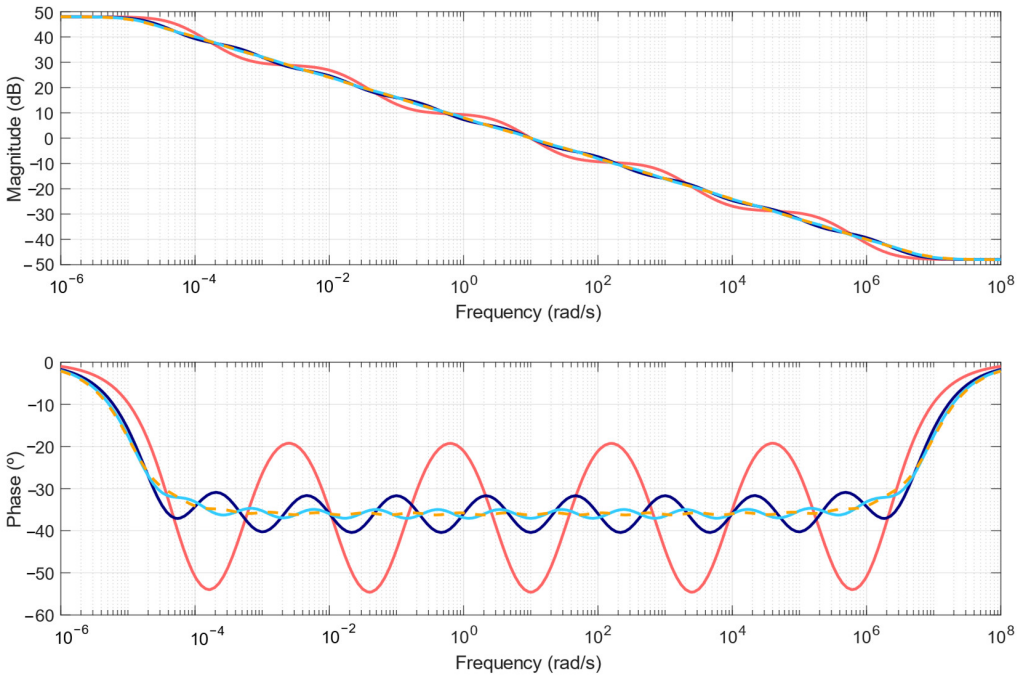

(b)

Figure 2. *Cont.*

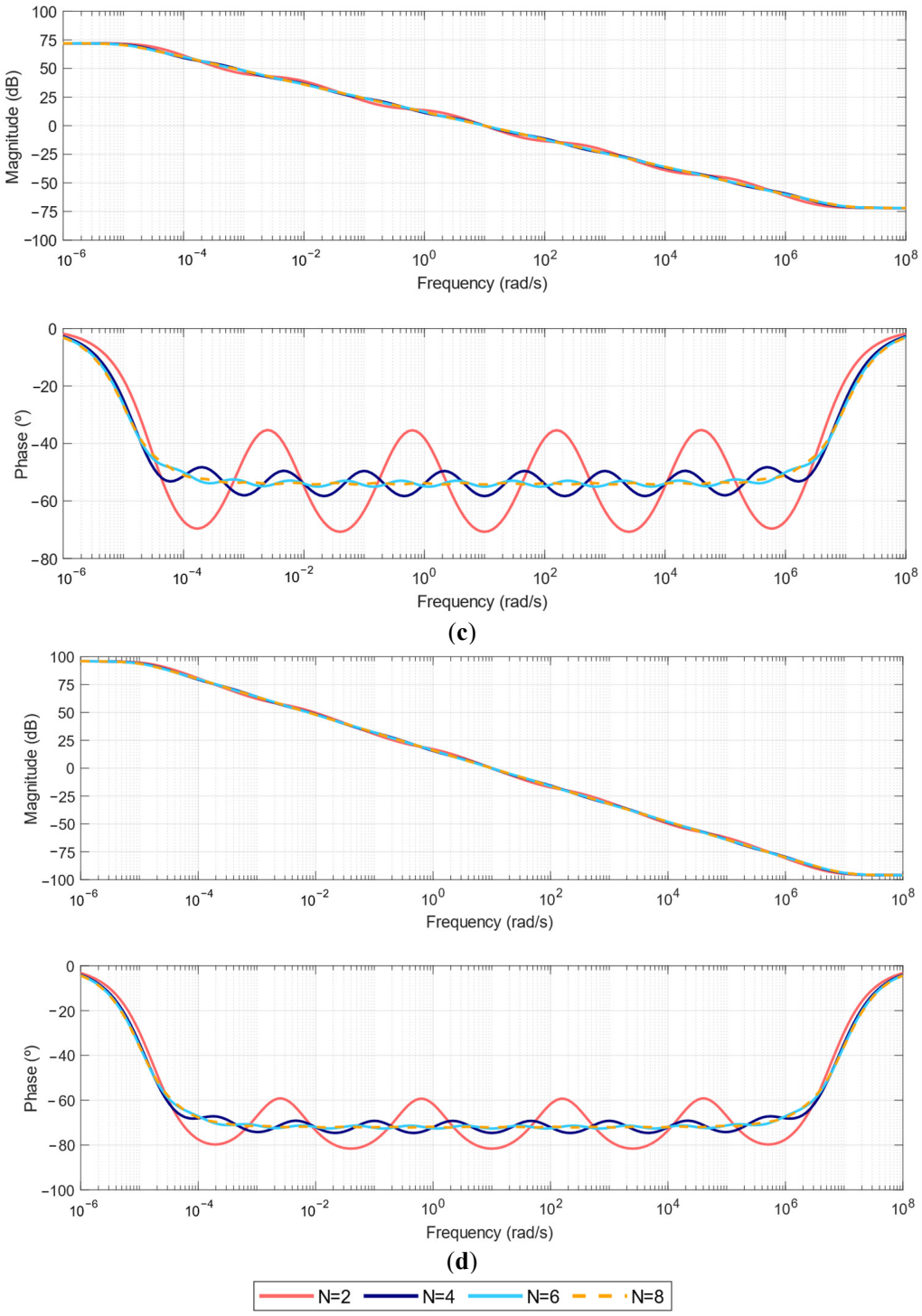

Figure 2. Approximation of (N = 2, 4, 5, 8) degrees of $s^{-\lambda}$ term, according to Oustaloup's recursive method, with: (**a**) λ = 0.2, (**b**) λ = 0.4, (**c**) λ = 0.6, and (**d**) λ = 0.8.

2.2. Fractional-Order Cascade Control for DC Motor Under Torque and Speed Steps

In this subsection, the system under study, i.e., the FOCS-based DC motor, is described. Its main controllers are fractional-order PI types. In Figure 3, the main schematic for such a system subjected to speed (ω_{ref}) and torque (T_L) steps is given.

In Figure 3, the cascade-based scheme can be identified along with current (internal) and speed (external) control loops, with each one dealing with the perturbations in either torque or speed steps, respectively. For each control loop, there is an associated PI controller.

In an IOCS-based DC motor, these PI controllers are of an integer-order nature and its governing equation in time domain is presented in (5) [38]:

$$y(t) = k_p e(t) + k_i \int_0^T e(t)dt \tag{5}$$

A PI controller is a type of controller that combines integral and proportional action, where y(t) represents the controller's output, e(t) the error, defined as the difference between the desired reference and the controller's output, and k_p and k_i are the controller's proportional and integral parameters. Furthermore, T is the time constant, which acts as the window of time in which the PI controller executes its actions. In the frequency domain, (5) is expressed in terms of the Laplace transform, whose equation is indicated in (6), and its main variables have been capitalized [38].

$$Y(s) = k_p E(s) + \frac{k_i}{s} E(s) = \left(k_p + \frac{k_i}{s}\right) E(s) \tag{6}$$

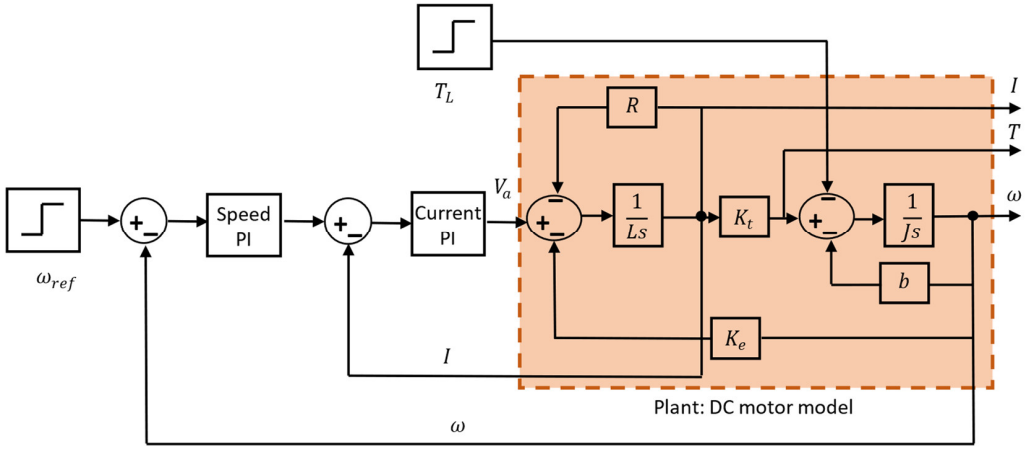

Figure 3. Cascaded scheme for speed and torque control of DC motor.

Cascade control schemes often include saturations in their PI controllers to prevent the drives from being damaged due the violation of their safe operational limits. Thus, the use of saturations limits the output of PI controllers, which is particularly important in DC motors, where excessive current can lead to overheating, mechanical stress, or even failure of the drive. By implementing saturations in PI controllers, these are forced to operate within predefined boundaries, which allows for system stability and protects the hardware. However, while saturation helps avoid damage, it can also provoke reduced responsiveness, slower settling times, or even oscillations, as the control action is no longer able to track the desired setpoint accurately. Therefore, whereas saturation can act as a safety measure, it can imply trade-offs between safety and optimal performance, which must be carefully considered in the design of the control system.

The equation in (6) yields the integer-order transfer function of a PI controller, $G_{IOPI}(s)$, expressed in (7) [38]:

$$G_{IOPI}(s) = \left(k_p + \frac{k_i}{s}\right) \tag{7}$$

In (7), the s^{-1} integrator is an integer-order term, and the present paper proposes substituting it by a fractional order term, $s^{-\lambda}$, where λ can range from 0 to 1. Therefore, λ represents an extra parameter that must be tuned in each current and speed PI controller of the cascade scheme to improve the DC motor behavior with respect to the IOCS-based DC

motor. The modified transfer function for each fractional-order PI controller, $G_{FOPI}(s)$, is presented in (8) [38].

$$G_{FOPI}(s) = \left(k_p + \frac{k_i}{s^\lambda}\right) \tag{8}$$

In (8), the s^λ term can be approximated with the method described in Section 2.1. It is the task of the present study to determine the combination adequacy of the fractional exponents of current (internal, λ_i) and speed (external, λ_e) PIs within the cascade structure to represent a global improvement over the IOCS-based DC motor.

The behavior of a DC motor can be understood through the interaction between its coupled electric and mechanic subsystems. When an external voltage is applied, it is distributed across the resistance (R), inductance (L), and counterelectromotive force ($k_e\omega$) of the DC motor. The resulting current (I) is responsible for the formation of the motor torque (T_M). In a steady-state regime, the DC motor reaches an equilibrium point, where the developed torque (T_M) compensates for the load torque (T_L) and friction losses. The rotor speed creates a counterelectromotive force ($k_e\omega$) that acts in feedback to oppose the applied voltage and limit the current.

In a study focused on the transient behavior of a DC motor, especially when controlled by a fractional-order cascade system, the inductance (L) cannot be neglected. During initial changes, such as the increase in applied voltage (V) or the increase in load torque (T_L), inductance introduces a delay in the current settling process. This delay is significant, as the current directly influences the development of the motor torque (T_M). Delays in current result in slower responses due to changes in torque or speed setpoints. Omitting the inductance's effect in the model would lead to an underestimation of the response times and a great part of the dynamic behavior, particularly during transient changes in speed or torque setpoints. Furthermore, with the presence of a fractional-order cascade control system, the inductance is crucial. Ignoring it would limit the controller's ability to manage efficiently the electric dynamics, as the integration of electric and mechanic dynamics becomes more accurate. In this context, inductance plays an important role in the current loop, which is the first loop to react against any system change. Furthermore, the rotor dynamics, affected by inertia and torque, are controlled by a speed loop that relies on the current loop, which is, in turn, influenced by the delay imposed by the inductance.

As for the equations of the DC motor, the transient model under the torque and speed steps is hereafter detailed in Equations (9)–(12), according to [34].

$$V(s) = RI(s) + LI(s)s + k_e\omega(s) \tag{9}$$

$$T_M(s) - T_L(s) = k_T I(s) - T_L(s) = J_r\omega(s)s + b\omega(s) \tag{10}$$

$$\omega(s) = \frac{1}{Js + b}(k_t I(s) - T_L(s)) \tag{11}$$

$$I(s) = \frac{1}{Ls + R}(V(s) - k_e\omega(s)) \tag{12}$$

In Equations (9)–(12), $V(s)$ represents the voltage applied to the stator,$I(s)$ the current that flows through it, and $\omega(s)$ is the speed of the rotor. As for torques, $T_M(s)$ is the torque developed by the DC motor and $T_L(s)$ is the load torque. Furthermore, R and L are the armature resistance and inductance, respectively, k_T and k_e are the torque and electromotive force parameters of the DC motor, and b and J are the friction coefficient and the rotor inertia, respectively.

3. Methodology

In this paper, the transient behavior of a FOCS-based DC motor under torque and speed steps is studied in comparison to that of the IOCS-based DC motor. In this sense, the λ_i and λ_e, the fractional exponents of current and speed PIs, respectively, have an impact on the transient behavior of the DC motor under torque and speed steps. This impact can be either beneficial or detrimental for the transient behavior of the DC motor, depending on how λ_i and λ_e, are combined within the cascade structure. Furthermore, a combination may improve certain aspects, such as rise time, but harm others, such as overshoot. To derive combination criteria for λ_i and λ_e, a methodological approach is defined subsequently. In Figure 4, the main flowchart for this methodology is presented, where the torque (T_L) and speed (ω_{ref}) steps are considered as influential inputs, as well as the DC motor model, whose equations define the plant to be controlled by the FOCS.

Furthermore, there is a set of metrics that represent different aspects of the transient behavior to be observed, which can be categorized into two groups:

- Overshoot, rise time, and peak current are key metrics evaluated under torque (T_L) and speed (ω_{ref}) step changes, with each metric associated with its respective variable, torque, or speed. Ideally, the overshoot, rise time, and peak current should be minimized compared to the performance of an IOCS-based DC motor.
- Peak torque and speed drop, however, are observed only under specific step changes: a peak in torque occurs as a transient response to a speed step, while speed drops occur in response to a torque step. These transients should be minimized, as they can destabilize the system mechanically, with the peak torque and speed drop posing particular challenges. Therefore, the occurrence of a torque peak in response to a speed step and a transient speed decrease in response to a torque step indicate coupling between the two variables. Optimizing the controller to mitigate these effects can be challenging, especially with fractional-order controllers, as each additional fractional parameter adds flexibility to the model, but also increases tuning complexity.

Therefore, the methodology starts with carrying out a preliminary study for the IOCS-based DC motor under torque and speed steps to select the basic current and speed PI parameters, i.e., of the proportional and integral types. These metrics will be considered for this preliminary study. Consequently, the results of this preliminary study are $\overrightarrow{K_{\substack{current\\loop}}}$ and $\overrightarrow{K_{\substack{speed\\loop}}}$, and the target time range during which the transient behavior of the IOCS-based DC motor under speed and a torque steps occurs.

According to the target time range obtained in the preliminary simulation of the IOCS-based DC motor, the polynomial order for the Oustaloup's recursive approximation method is selected to cover it with sufficient accuracy. For this purpose, a comparative analysis is performed through bode diagrams for different polynomial degrees and fractional orders. With this information, the FOCS is built according to Oustaloup's recursive method.

Simulations of the FOCS-based DC motor are conducted in MATLAB–SIMULINK, by preserving the same proportional and integral control parameters in both the current and speed PIs, as in the preliminary integer-order study. As a result, different improvements in and preservations and deteriorations of the DC motor metrics are observed with respect to the thresholds obtained in the IOCS-based DC motor. To analyze the influence of λ_i and λ_e, pairing criteria for these fractional exponents are established through bar charts to improve, or at least preserve the performance of the IOCS-controlled DC motor, based on predefined metrics under torque and speed steps, separately. Therefore, there will be an acceptable range, R_k, of λ_i and λ_e pairings for each metric, k, which implies an improvement in or preservation of a metric result with respect to the IOCS-controlled DC motor, which is represented with a threshold, Th_k. These ranges are commented on for each type of input,

whether a speed step or a torque step. It is important to note that, among these metrics, the rise time, overshoot, and peak current in the behavior of the DC motor are analyzed under both torque and speed steps. However, there are other metrics, such as the transient peak torque that occurs during a speed change or the transient speed drop that occurs during a torque change.

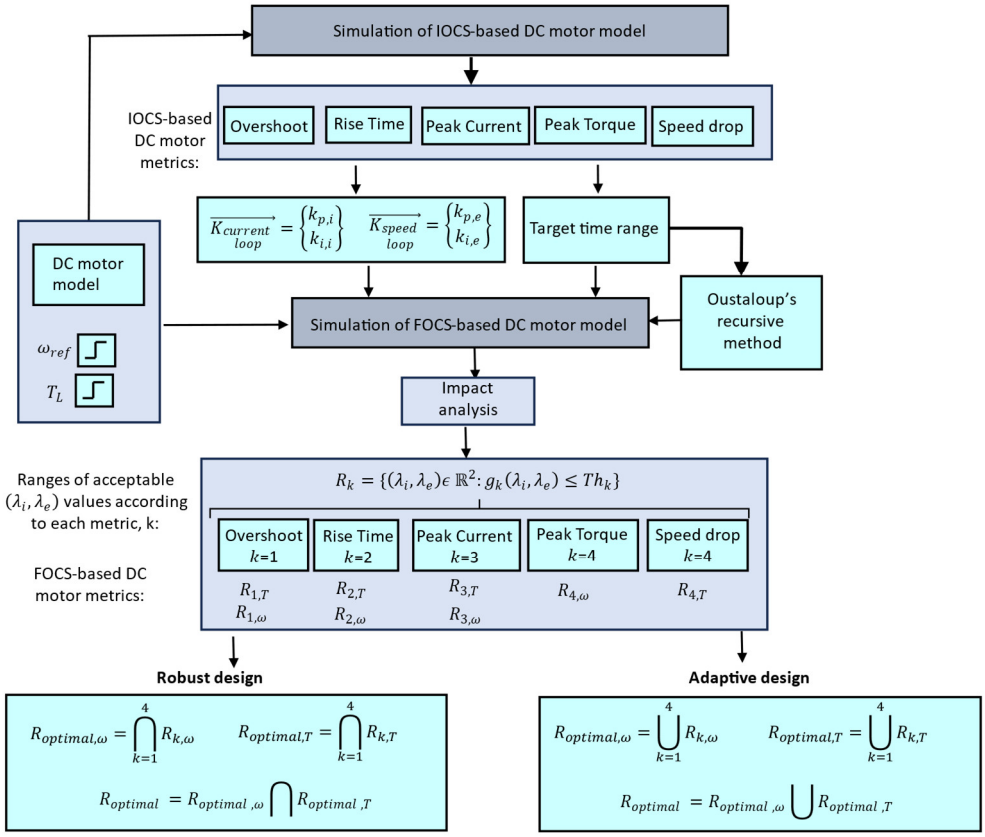

Figure 4. Methodology flowchart.

Combination criteria are derived from this analysis for each metric individually and represented in 3D plots. Through these 3D plots, pairings of λ_i and λ_e are proposed to improve each metric separately with respect to the result obtained with the IOCS-based DC motor.

The results are summarized in two maps: one for the DC motor's behavior under the predefined speed step, and another under the predefined torque step. These maps help to identify suitable λ_i and λ_e combinations to optimize multiple metrics simultaneously by intersecting acceptable ranges, supporting robust design. Alternatively, they represent the union of λ_i and λ_e values for adaptive control, allowing dynamic adjustment of priorities and tuning of λ_i and λ_e based on the control objectives in different scenarios.

To extend the derived criteria to other torque and speed steps that involve more profound changes, an additional analysis is included to detect critical pairings of fractional exponents that would worsen in a more significant way the DC motor's behavior.

4. Preliminary Integer-Order Cascaded Control for DC Motor

In Table 2, the physical parameters that define the DC motor model under study are enclosed.

Table 2. Physical parameters of the DC motor under study.

Parameter	Symbol	Value	Parameter	Symbol	Value
Rated Voltage (V)	U_r	24	Electromotive Force Parameter (Vs/rad)	k_e	6.5×10^{-2}
Rated Speed (rpm)	ω_r	3000	Torque Parameter (Nm/A)	k_T	5.3×10^{-2}
Rated Current (A)	I_{rated}	47	Armature Resistance (Ω)	R	0.21
Rated Torque (Nm)	T_{rated}	0.353	Inductance (mH)	L	0.51
Rotor Inertia (kgm^2)	J	4×10^{-5}	Viscous Friction Coefficient (Nms)	b	2×10^{-4}

It is well known that within a nested control scheme, the time constant of speed (external) loop, T_e, must exceed several times that of the current (internal) loop, T_i, to avoid undesired behavior. However, depending on the plant to be controlled and the application characteristics, T_e/T_i may adopt different values within the range of 1 to a 12.

Therefore, the objective of this section is to carry out a preliminary study for an IOCS-based DC motor using different T_e/T_i values to determine the most appropriate T_e/T_i ratio for the given application. In Table 3, the integral ($k_{i,i}, k_{i,e}$) and proportional ($k_{p,i}, k_{p,e}$) parameters of both current and speed loops are enclosed for each T_e/T_i relationship.

Table 3. Internal–external loop relationships for integer-order cascaded control.

T_e/T_i	Current (Internal) PI Loop Parameters		Speed (External) Loop Parameters	
	$k_{p,i}$	$k_{i,i}$	$k_{p,e}$	$k_{i,e}$
10	1	100	1	10
3	10	78.125	1.386	3.61
2.22	4.158	72.18	2	15.625
1	10	100	1	10

In Figure 5, the simulation results for the IOCS-based DC motor are extracted under a speed change (Figure 5a–c) and under a torque change (Figure 5d–f) with different proposals for T_e/T_i ratios. The speed change is characterized by a speed step from 95% to 100% of the rated speed, whereas the torque change is characterized by a change from 50% to 100% of the rated torque.

For the system under the aforementioned speed step, the evolution of the transient speed (Figure 5a), the transient peak torque affected by the speed step (Figure 5b), and the transient I/I_{rated} ratio (Figure 5c) are presented. Analogously, for the system under the aforementioned torque step, the evolution of the transient torque (Figure 5d), the speed affected by the torque step (Figure 5e), and the transient I/I_{rated} ratio (Figure 5f) are presented. The curves in dashed lines are the setpoints to be met.

By considering only the performance of the DC motor under a speed setpoint change, it can be deduced from Figure 5a that T_e/T_i = 2.22 is the proposal that most rapidly makes the speed reach the setpoint without overshoot. The rest of the proposals for T_e/T_i imply a slower convergence to the speed setpoint. However, there is a transient peak on the torque affected by the speed change that differs according to the T_e/T_i ratio. For T_e/T_i = 10, the peak presents its minimum value, while for T_e/T_i = 2.22, it reaches its maximum. The rest of the proposals lie within the mentioned limits. The transient I/I_{rated} ratio displays similar behavior, adopting a maximum peak for T_e/T_i = 2.22 and a minimum peak for T_e/T_i = 10. By considering only the performance of the DC motor under a torque setpoint change, as shown in Figure 5d, T_e/T_i = 2.22 is the proposal that most rapidly makes the torque reach the setpoint without overshoot. The rest of the proposals for T_e/T_i make the torque converge to the setpoint more slowly, and even with overshoot for I/I_{rated} = 10.

However, there is a transient speed drop provoked by the torque change that differs according to the T_e/T_i ratio. For T_e/T_i = 10, the peak presents its greatest depth, while for I/I_{rated} = 2.22, the peak reaches its minimum depth. The rest of the proposals lie within the mentioned limits.

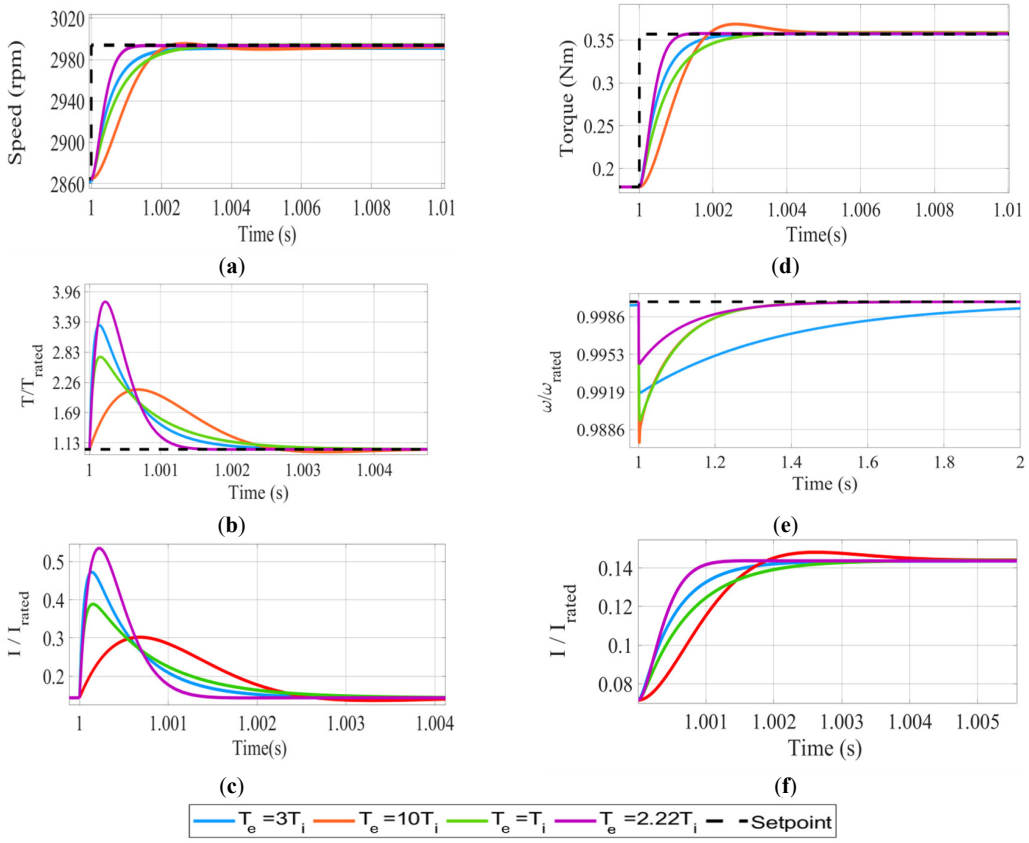

Figure 5. For the different T_e/T_i ratios, evolution of different variables under the predefined speed step change: (**a**) transient speed (rpm), (**b**) transient torque (Nm), and (**c**) transient I/I_{rated}. Evolution of different variables under the predefined torque step change: (**d**) transient torque (Nm), (**e**) transient speed (rpms), and (**f**) transient I/I_{rated}.

The transient I/I_{rated} signal of the DC motor under the torque step follows different behavior from that observed when subjected to the speed step. Under the torque step, the I/I_{rated} ratio presents linear transient behavior and stabilizes rapidly overall. For I/I_{rated} = 2.22, the signal reaches the lowest rise time, and for either lower or greater values than 2.22, the rise time for I/I_{rated} reaches greater values.

Therefore, although the behavior of the DC motor under both speed and torque changes is optimal for I/I_{rated} = 2.22, such parameterization poses other disadvantages, such as having the greatest transient current and torque peaks during speed changes, among all the selected proposals.

This means that there is room for improvement for the IOCS-based DC motor behavior under speed changes that can be covered by a FOCS. However, and as will be shown in the FOCS-based analysis, there is also room for worsening the IOCS-based DC motor's behavior. This study concludes with the final selected T_e/T_i = 2.22, with parameters of $k_{p,e}$ = 2, $k_{i,e}$ = 15.625 and $k_{p,i}$ = 4.158, $k_{i,i}$ = 72.18. The corresponding values associated with the different metrics of the IOCS-controlled DC motor behavior under a speed and a torque step are summarized in Table 4. These values will define the different thresholds for comparison in next section within each metric.

Table 4. Results of different metrics of the IOCS-controlled DC motor under a speed and a torque step.

	Rise Time (μs)	**Overshoot (%)**	**I/I_{rated}**	**T/T_{rated}**	**ω/ω_{rated}**
Speed step	624	0.00826	0.53	3.77	
Torque step	624	0.2016	0.145		0.9944

5. Fractional-Order Cascade Control for DC Motor

In this section, a FOCS-based control for the DC motor is explored for different λ_e and λ_i values and compared with the IOCS-based DC motor in Figures 6 and 7, when subject to the speed and torque steps defined in Section 4, respectively. The proportional and integral control parameters of the FOPIs are preserved with respect to the chosen parameters in the previous section. The FOCS-based DC motors are characterized by the following:

- λ_e = 0.1 and λ_i = 0.9, which improves the IOCS-based DC motor behavior in terms of the rise time during speed and torque steps (160 vs. 624 μs). However, it worsens the IOCS-based DC motor behavior in terms of oscillation (1% vs. 0.00826%), peak current (1.37 vs. 0.53 times the rated current), and torque (9.71 vs. 3.77 times the rated torque) during the speed step. It also worsens the behavior in terms of oscillation (15% vs. 0.206%) and peak current (0.164 vs. 0.145 times the rated current) during the torque step. It presents a similar transient speed drop during the torque step (0.998 vs. 0.9944 the rated speed value).
- λ_e = 0.4 and λ_i = 0.6, which improves the IOCS-based DC motor behavior in terms of the rise time (410–481 vs. 624 μs) during both speed and torque steps. In turn, it presents worse behavior than that of the IOCS-based DC motor in terms of the oscillation level during the speed (0.292 vs. 0.00826%) and torque steps (4.63 vs. 0.2016%), peak current (0.64 vs. 0.53 times the rated current value), and torque (4.53 vs. 3.77 times the rated torque value) during the speed steps. During the torque step, the transient peak current is within a similar range compared with the IOCS-based DC motor (0.15 vs. 0.145%), as well as the speed drop (0.9953 vs. 0.9944 times the rated speed value).
- λ_e = 0.9 and λ_i = 1, which implies very similar behavior to the IOCS-based DC motor. Similar rise times during both the speed and torque steps (623.9 vs. 624 μs), as well as similar oscillation levels during both the speed (−0.0078 vs. 0.00826%) and torque steps (0.332 vs. 0.2016%), are observed. The peak current (0.536 vs. 0.53 times the rated current value) and peak torque (4.2 vs. 3.77 times the rated torque value) levels during the speed step also adopt similar, albeit higher values compared to the IOCS-based DC motor. The transient speed drop during the torque step also presents a similar value (around 0.995 times the rated speed), which is also the case for the transient peak current value (0.14 times vs. 0.143 the rated current), as with the IOCS-based DC motor.

It can also be seen that the IOCS-based DC motor always presents the closest responses to the reference values when reaching the steady-state regime, compared to the FOCS-based DC motors.

Although clear improvements in rise time can be extracted from the FOCS-based compared to the IOCS-based DC motor, there are still metrics that cannot be improved simultaneously, and that may require different λ_e and λ_i values according to the optimization objective. Therefore, to understand better the influence of the λ_e and λ_i values on the DC motor performance within a cascade scheme, an impact analysis is developed in the next section.

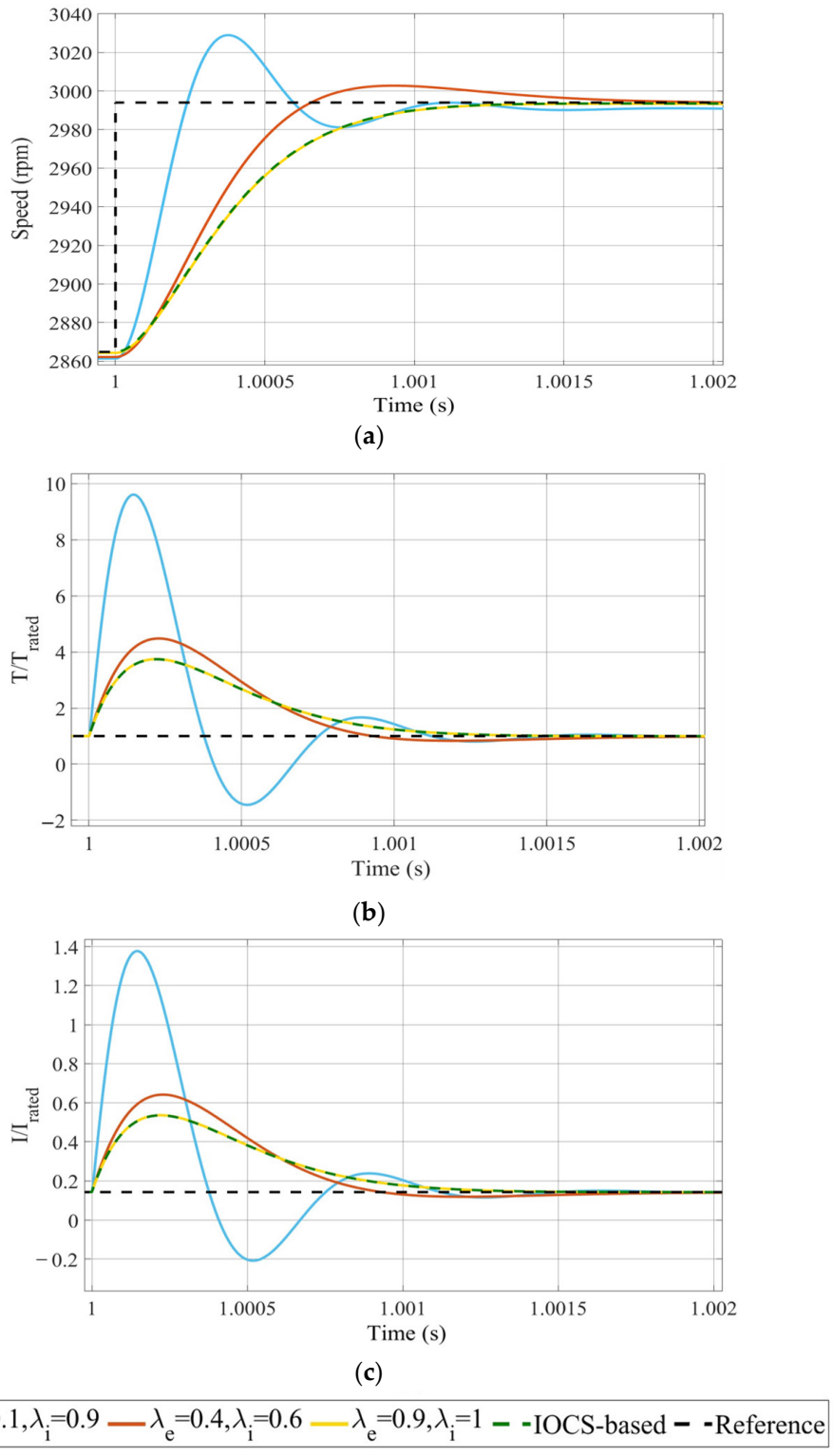

Figure 6. For the different FOCS-based DC motors, evolution of different variables under the predefined speed step (95% to 100% of rated speed): (**a**) speed (rpm), (**b**) T/T_{rated}. (Nm), and (**c**) I/I_{rated}.

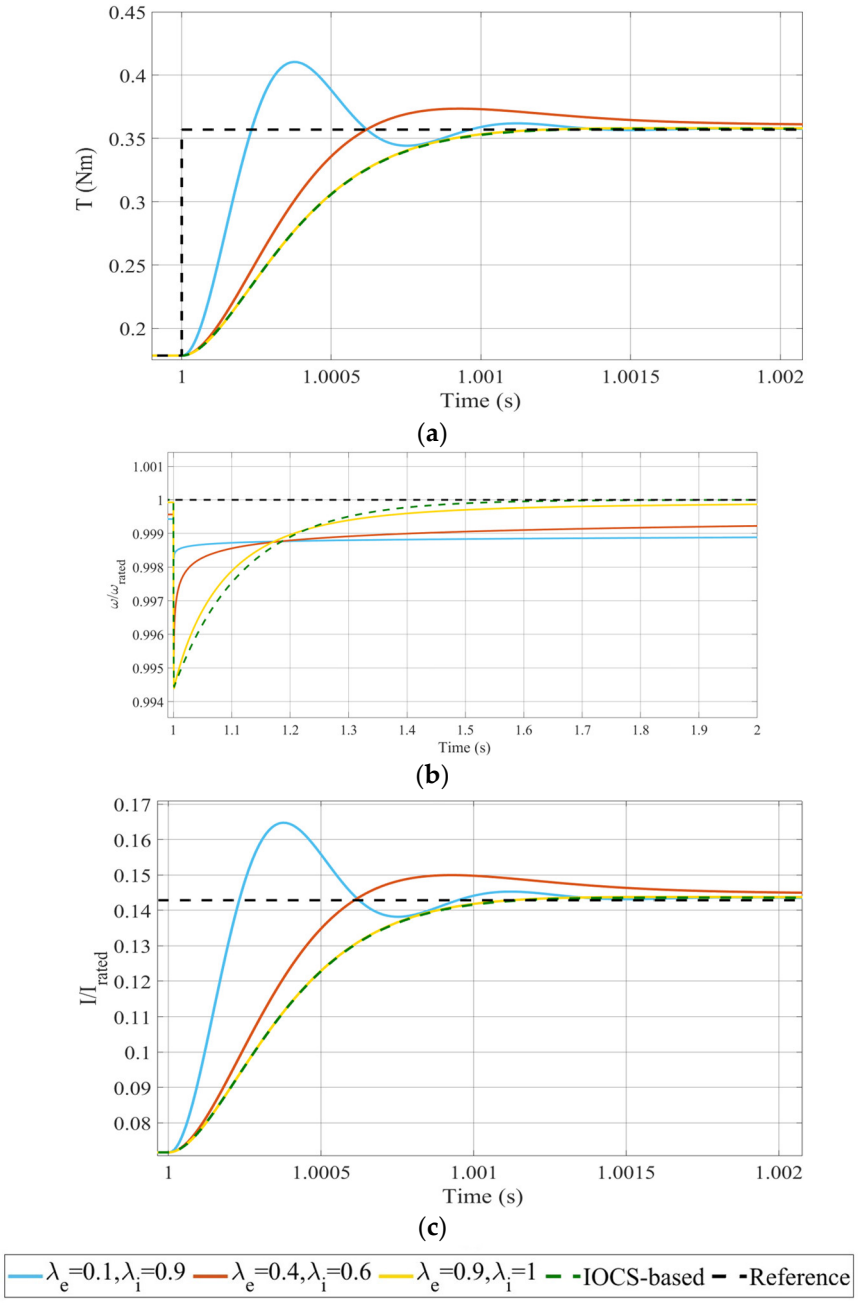

Figure 7. For the different FOCS-based DC motors, evolution of different variables under the prodefined torque step (0% to 100% of rated torque): (**a**) torque (Nm), (**b**) ω/ω_{rated} (Nm), and (**c**) I/I_{rated}.

6. Impact Analysis

In this section, the FOCS-based DC motor is analyzed for different combinations of fractional orders, λ_e and λ_i, under torque and speed steps. The section starts with a predefined T_e/T_i = 2.22, with specific parameters discussed in Section 4 to understand better the simulations in Section 5 and derive the pairing criteria of λ_e and λ_i according to the desired metrics. For this purpose, Section 6 is divided into three parts: in Section 6.1, the influence of λ_e and λ_i on the metrics is clarified, while in Section 6.2, the pairing criteria for λ_e and λ_i to improve the behavior of the equivalent IOCS-based DC motor are discussed according to each metric. In Section 6.3, performance evaluation maps are presented and robust/adaptive design implications are derived.

6.1. Influence of Speed (λ_e) and (λ_i) Fractional-Order Loops

The influence of λ_e and λ_i on the speed rise time, overshoot, transient current peak, and torque peak under the predefined speed step are shown in Figure 8a–d, respectively, whereas the impact of λ_e and λ_i on the torque rise time, overshoot, transient current peak, and speed drop under the predefined torque step are shown in Figure 9a–d, respectively. The λ_e and λ_i values have been selected within the range of 0 to 1 in intervals of 0.1. In every single subfigure, there is a dashed black line that comes from the result of the IOCS-based DC motor. This level acts as a threshold to determine whether λ_e and λ_i improves or worsens the IOCS-based DC motor behavior.

As for the rise time, the mark reached by the IOCS-based DC motor is 624 µs in both speed and torque signals subjected to the predefined steps. The reduction in λ_e helps to reduce this mark further, reaching a minimum of 250 µs with λ_e = 0.6 and 100 µs with λ_e = 0.1, while closer λ_e values to 1 are near the IOCS-based DC motor mark. In contrast, λ_i does not have such a significant effect on the rise time as λ_e. Anyway, there are low values of λ_i ($\lambda_i \leq 0.3$) paired with high values of λ_e ($\lambda_e \geq 0.5$) that worsen the rise time of the IOCS-controlled DC motor. Values of λ_e and λ_i outside this range improve the rise time of the IOCS-based DC motor.

As for the overshoot level, the marks reached by the IOCS-based DC motor are 0.2016% under the torque step and 0.00826% under the speed step. Regardless, the variation patterns caused by the fractional exponents in the overshoot levels under either speed or steps are similar, as can be seen in Figures 8b and 9b, although within the speed step, there are negative oscillation levels, which indicate that the signal never exceeds the reference. There is a range defined for each λ_i value, so that $\lambda_e \geq 0.6$ for the speed step and $\lambda_e \geq 0.8$ for the torque step, where the oscillation levels are lower than or similar to those in the IOCS-based DC motor. Outside this range, the impact of λ_e on the overshoot level is such that its increment implies greater overshoot levels than in the IOCS-based DC motor.

The λ_e and λ_i orders present different impact patterns when subjected to the speed and torque steps. Under the speed step, there are no damping capabilities for this transient current peak, as both λ_e and λ_i exponents provide similar or worse transient peak levels compared with the IOCS-based DC motor. The same happens with the transient torque peak under the speed step, as shown in Figure 8d. However, during the torque step, the peak current for $\lambda_e \geq 0.6$ for each λ_i is similar to or lower than that with the IOCS-based DC motor. Outside this range, the current peak adopts greater values than that from the IOCS-based DC motor, as shown in Figure 9c. On the other hand, the torque overshoot and torque ripple are interconnected, as they exhibit mutually influential behavior. In this sense, the torque overshoot during a transient period may influence the steady-state DC motor's behavior and promote torque ripple under certain conditions. Furthermore, a transient torque overshoot may cause current oscillations, which could be extended in time, or even allow for harmonic content, which can contribute to torque ripple formation. Furthermore, the presence of torque ripple may affect and increase the transient overshoot by posing an extra difficulty in the accurate control of the DC motor.

In Figure 9d, the speed drop obtained due to the torque step is analyzed throughout the different values of λ_e and λ_i. Any fractional exponent improves this mark as it makes the speed drop less deep than with the IOCS-based system under the torque step, although the values are very similar. However, the deeper the speed drop, the more time the DC motor will need to recover its rated value.

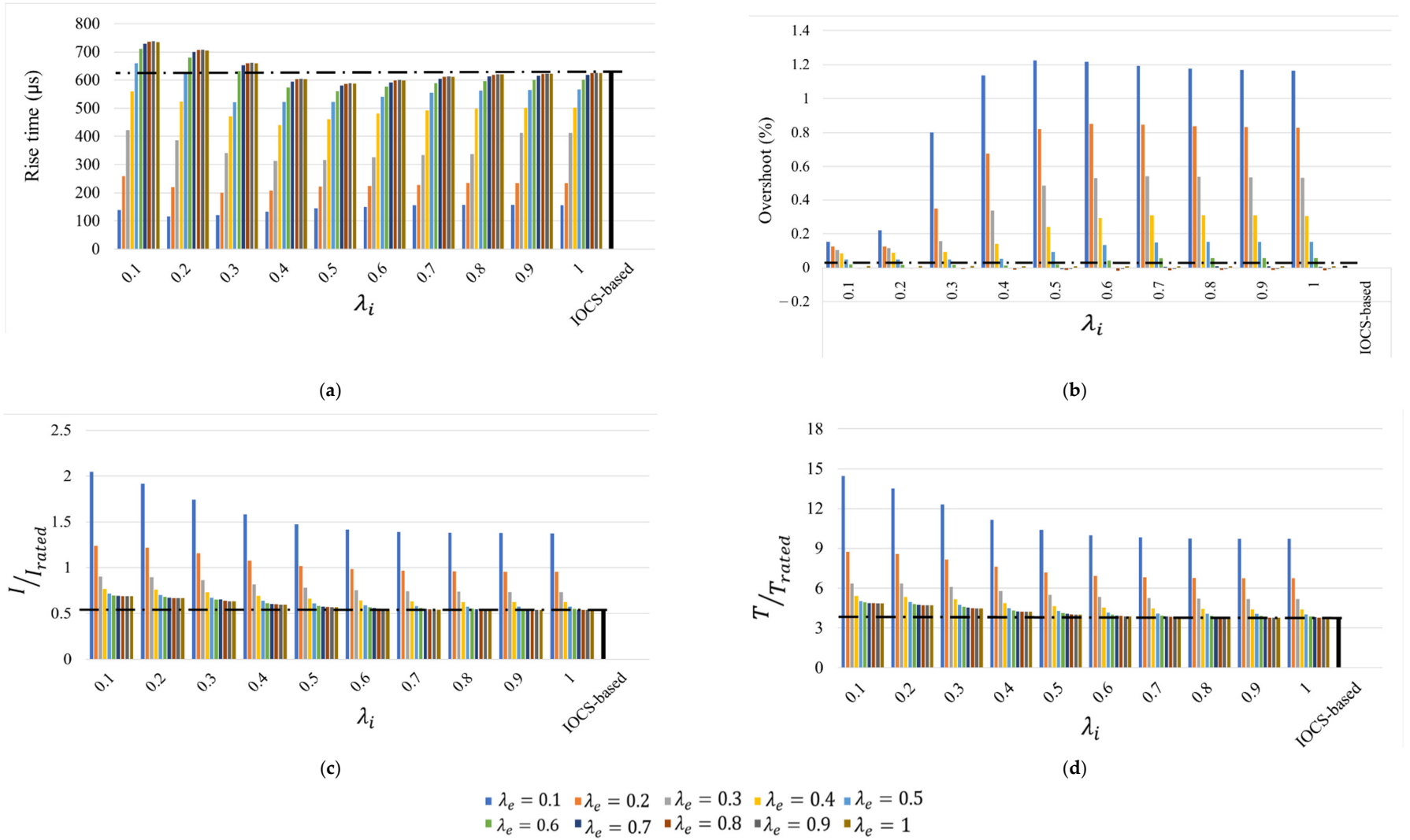

Figure 8. Impact of different λ_i and λ_e values on the metrics of the FOCS-based DC motor under the predefined speed step (95% to 100% of the rated speed value): (**a**) rise time (μs) of speed signal, (**b**) overshoot (%) of speed signal, (**c**) peak current due to the speed step and (**d**) peak torque due to the speed step. The black dashed lines in subfigures pinpoint the results of the IOCS-based DC motor.

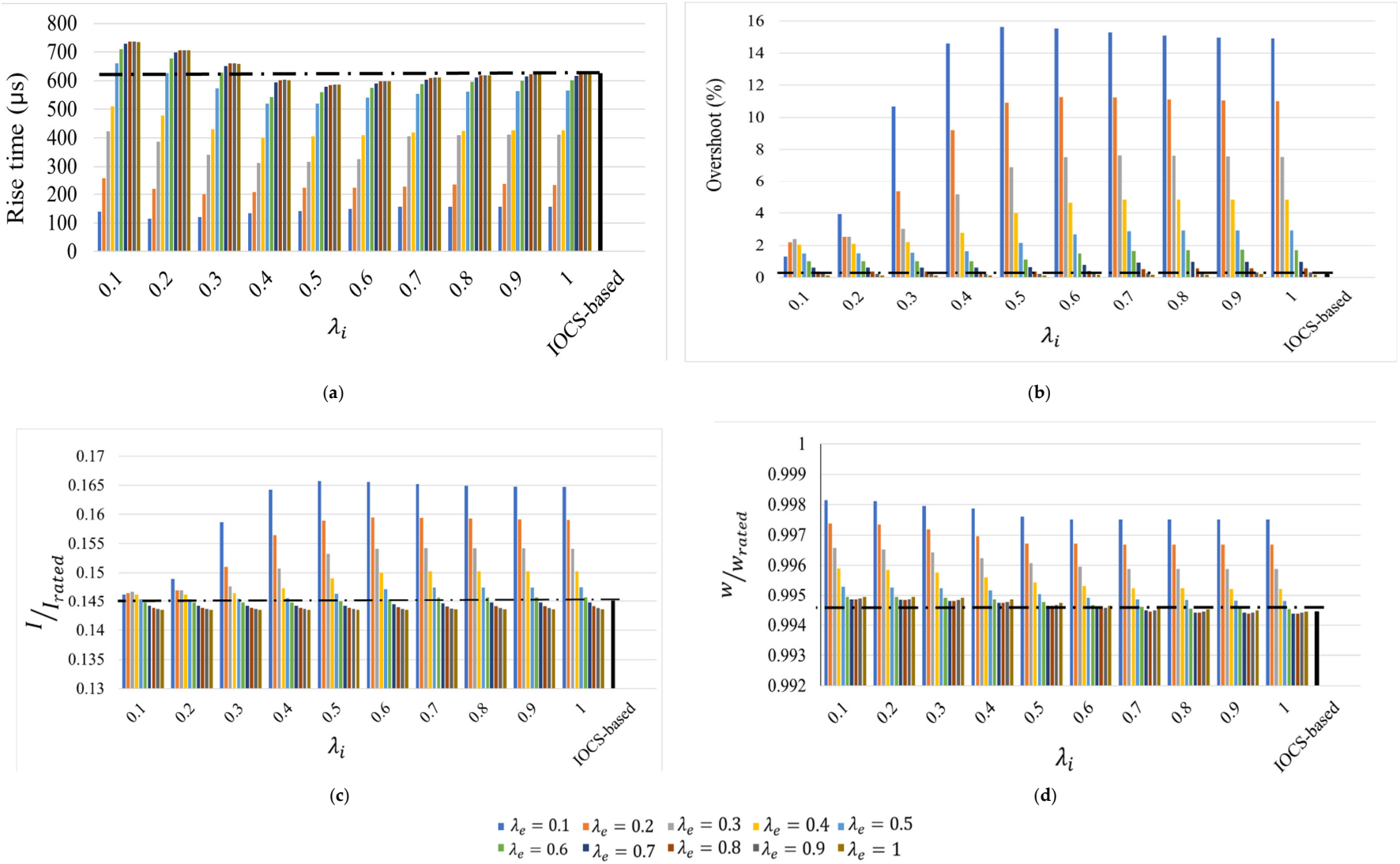

Figure 9. Impact of different λ_i and λ_e values on the metrics of the FOCS-based DC motor under the predefined torque step (from 50% to 100% the rated torque value): (**a**) rise time (µs) of torque signal, (**b**) overshoot (%) of torque signal, (**c**) peak current due to the torque step and (**d**) speed drop due to the torque step. The black dashed lines in subfigures pinpoint the results of the IOCS-based DC motor.

6.2. Pairing Criteria to Improve the IOCS-Controlled DC Motor

Therefore, the criteria for pairing λ_e and λ_i to improve the behavior of the FOCS-based over the IOCS-based DC motor are summarized in Figures 10 and 11, according to different metrics. The pairing criteria for such improvements under the speed step are shown in Figure 10, and those for improvements under the torque step are shown in Figure 11. The areas in dark red in Figures 10 and 11 represent similar or worse metric levels compared with the IOCS-based DC motor, while the areas in blue represent similar or better levels. In this sense, greater rise time, overshoot, and peak and torque levels are detrimental, whereas a more superficial speed drop during the torque step is beneficial.

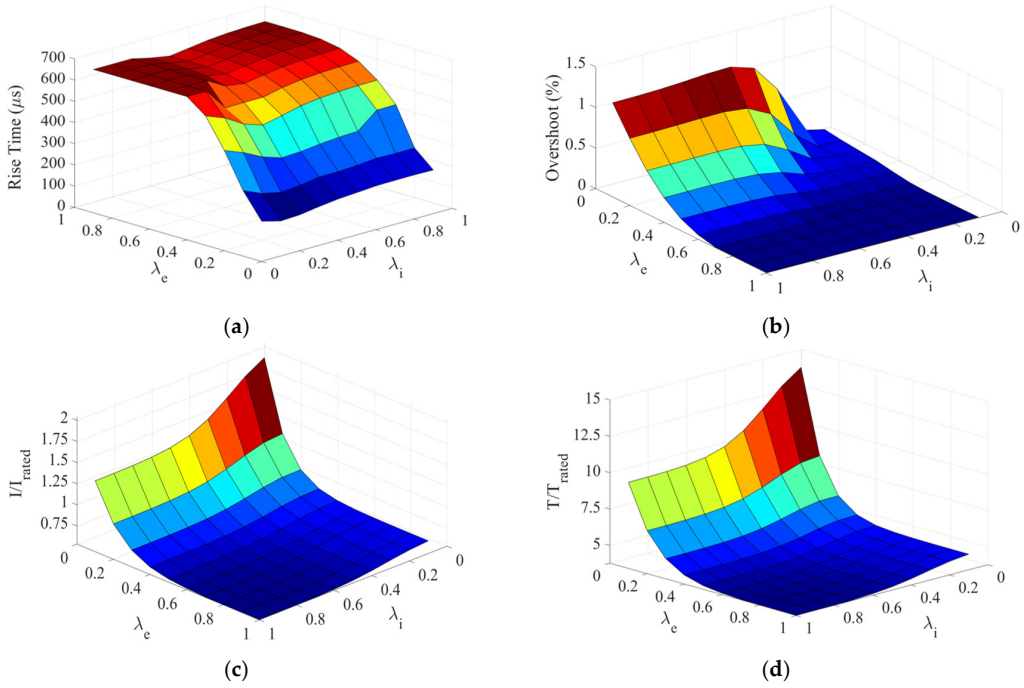

Figure 10. Pairing criteria of λ_e and λ_i for a FOCS-based DC motor under the predefined speed step, namely from 95% to 100% of speed torque, to allow for improvements in different criteria with respect to the IOCS-based DC motor: (**a**) rise time (μs) of speed signal, (**b**) overshoot (%) of speed signal, (**c**) peak current due to the speed step, and (**d**) peak torque due to the speed step. The areas in dark red represent similar or worse metric levels compared with the IOCS-based DC motor, while the areas in blue represent similar or better levels.

As for the rise time and oscillation values, λ_e has a greater impact overall than λ_i on reducing both the rise time and the overshoot level under both torque and speed steps with respect to the IOCS-based DC motor. Reducing λ_e is the best action to improve the rise time levels of the IOCS-based DC motor during both the speed and torque steps. However, for the oscillation levels during torque and speed steps, the best combination is made of high λ_e values.

As for the transient peak current, in case of the torque step, the FOCS-based systems with large $\lambda_e \geq 0.6$ values allow for peak current reduction with respect to that of the IOCS-based DC motor for each λ_i, while the λ_e and λ_i values outside this range are discarded, as they present greater peak current. For the speed step, the transient peak current and torque values are always greater than that of the IOCS-based DC motor, and, therefore, there is no room for improvement. However, if these metrics are critical, λ_e and λ_i values close to 1 will imply similar peak torque and peak current values as those with the IOCS-based DC motor. As for the speed drop caused by the torque step, this can be similar or reduced by each single combination of λ_e and λ_i with respect to that of the IOCS-based DC motor.

In other works, such as [13], the proportional, integral, and derivative control parameters are tuned for servo systems, along with the fractional orders of primary and secondary

loops. However, the chosen fractional orders are not decoupled from the proportional and integral control parameters, as was undertaken in the present article, to discern the beneficial or detrimental effects of pairing fractional exponents.

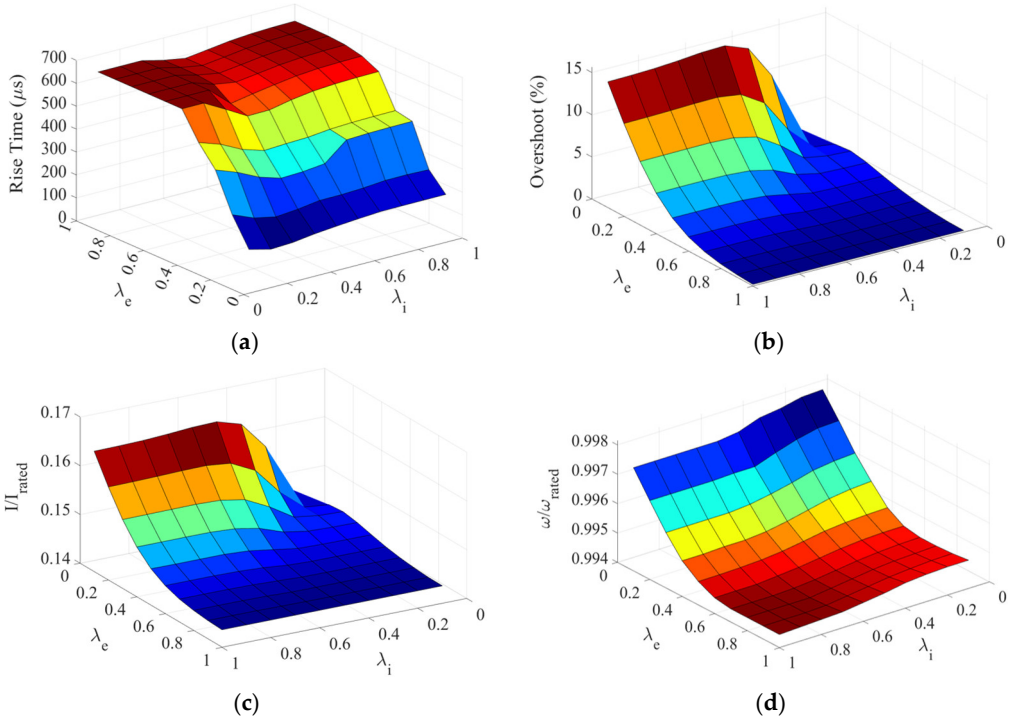

Figure 11. Pairing criteria of λ_e and λ_i for a FOCS-based DC motor under the predefined torque step from 50% to 100% of nominal torque, to allow for improvements in different criteria with respect to the IOCS-based DC motor: (**a**) rise time (μs) of torque signal, (**b**) overshoot (%) of torque signal, (**c**) peak current due to the torque step, and (**d**) speed drop due to the torque step. The areas in dark red represent similar or worse metric levels compared with the IOCS-based DC motor, while the areas in blue represent similar or better levels.

The developed study in the present paper is similar to that in [39], in which a trade-off analysis between rise time, overshoot, torque ripple, and commutation frequency was developed for a five-phase induction motor. In that study, as well as in the present study, improvements in several metrics, such as overshoot and torque ripple, were not possible at the same time. Furthermore, both articles highlight the presence of coupled variables between the speed (external) and current (internal) loops. In this sense, the peak torque during a speed step or the speed drop during a torque step are examples of the aforementioned coupled mechanic and electric loops and, thus, a consequent pairing must be guaranteed. Furthermore, the operational point also plays an important role, as commented on in [39], and as will also be discussed in Section 7. Furthermore, in [31], the proposed trade-off analysis is also supported by a Pareto analysis, and similar conclusions are obtained to those in [39].

6.3. Performance Evaluation Maps and Robust/Adaptive Design Implications

In Figures 10 and 11, the criteria for pairing λ_e and λ_i are derived according to separate metrics, as far as they represent a behavior improvement over the IOCS-based DC motor. However, for many metrics, the pairing of λ_e and λ_i did not exhibit a straightforward pattern, nor did it guarantee the simultaneous improvement or preservation of other metrics. Therefore, the maps in Figures 12 and 13 make it possible to deduce the set of λ_e and λ_i values to define either a robust control design to optimize different metrics simultaneously for the FOCS-based DC motor, or to propose an adaptive control design in which λ_e and λ_i values can be dynamically adjusted, depending on the priorities of

different operational scenarios. The maps in Figures 12 and 13 reflect the aforementioned design implications for pairing the fractional orders under the speed and torque steps, respectively. Such maps provide graphical information only for the λ_e and λ_i values that improve the behavior of the FOCS-based over the IOCS-based DC motor according to the different criteria. In this way, those cells that correspond to different pairings of λ_e and λ_i values have been filled with different patterns if they improve or preserve the different metrics. The meaning of each pattern is summarized below:

- The cells filled with horizontal lines correspond to those pairings that improve the rise time of the FOCS-based with respect to the IOCS-based DC motor.
- The cells filled with an orange pattern represent the pairings that improve the overshoot level of the FOCS-based with respect to the IOCS-based DC motor.
- The cells filled with vertical lines correspond to those pairings that improve the transient peak current level of the FOCS-based with respect to the IOCS-based DC motor.
- The cells filled with a blue pattern indicate the cross-influence variable. In Figure 12, this corresponds to the transient peak torque during the speed step, while in Figure 13, it represents the transient speed drop during the torque step. Accordingly, the blue-highlighted cells identify pairings that enhance the value of this cross-influence metric in the FOCS-based DC motor compared to the IOCS-based counterpart.
- The black cell in each graph corresponds to the IOCS-based DC motor.

Additionally, the more patterns are present inside a cell, the greater the number of metrics that are improving or preserving the specific pairing of λ_e and λ_i values. The crosses indicated in both figures pinpoint the previous simulated FOCS-based DC motor models with specific pairings of λ_e and λ_i values.

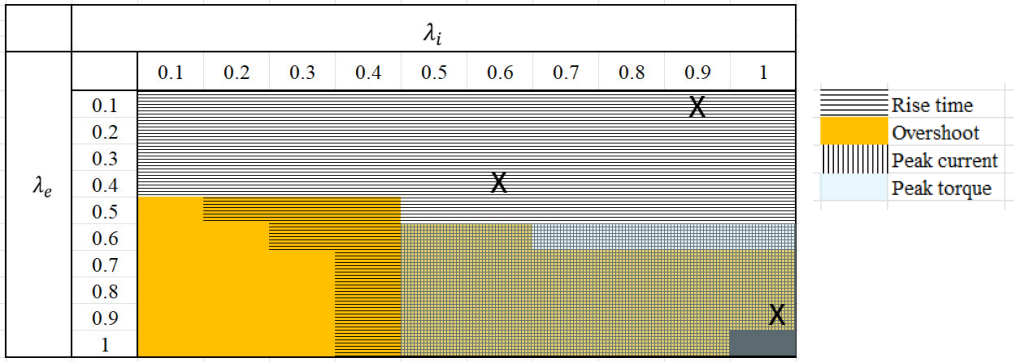

Figure 12. For a FOCS-based DC motor under the predefined speed step, performance evaluation maps for pairing fractional orders according to different metrics.

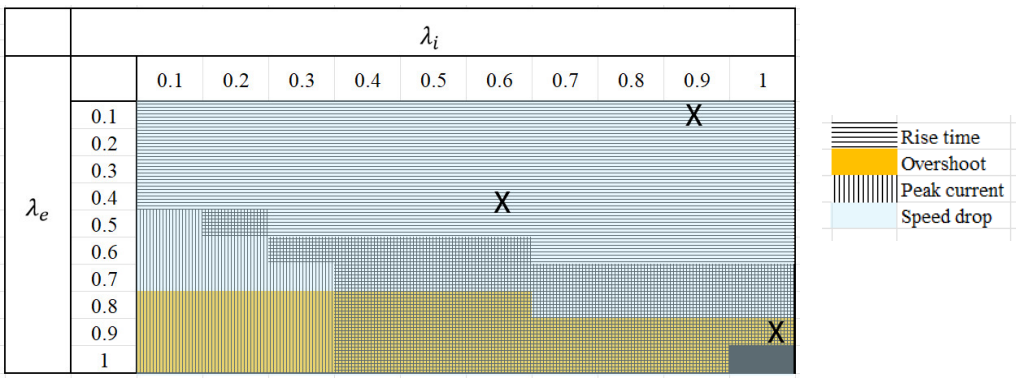

Figure 13. For a FOCS-based DC motor under the predefined torque step, performance evaluation maps for pairing fractional orders according to different metrics.

Therefore, the main pairing criteria can be summarized in two points:

- For a robust design, in which the ranges of λ_e and λ_i values are intersected to improve or preserve metrics simultaneously, the final range will be the square area defined by the following corners:
  - Under a speed step
    (λ_i, λ_e): (0.5, 0.6), (0.6, 0.6), (0.7, 0.7), (1, 0.7), (1, 0.9), (0.9, 1), (0.5, 1).
  - Under a torque step
    (λ_i, λ_e): (0.4, 0.8), (0.6, 0.8), (0.7, 0.9), (1, 0.9), (0.9, 1), (0.4, 1).
  - Robust design
    (λ_i, λ_e): (0.5, 0.8), (0.6, 0.8), (0.7, 0.9), (1, 0.9), (0.9, 1), (0.5, 1).
- For an adaptive design, to improve the following metrics, different areas are defined by the following corners:
  - To improve the rise time under speed or torque step
    (λ_i, λ_e): (0.1, 0.1), (1, 0.1), (1, 0.9), (0.9, 1), (0.4, 1), (0.4, 0.7), (0.3, 0.6), (0.2, 0.5), (0.1, 0.4).
  - To improve or preserve overshoot under a speed step
    (λ_i, λ_e): (0.1, 0.5), (0.4, 0.5), (0.5, 0.6), (0.6, 0.6), (0.7, 0.7), (1, 0.7), (1, 0.9), (0.9, 1), (0.1, 1).
  - To improve or preserve overshoot under a torque step
    (λ_i, λ_e): (0.1, 0.8), (0.6, 0.8), (0.7, 0.9), (1, 0.9), (0.9, 1), (0.1, 1).
  - To improve or preserve the transient peak current and peak torque under a speed step:
    (λ_i, λ_e): (0.5, 0.6), (1, 0.6), (1, 0.9), (0.9, 1), (0.5, 1).
  - To improve or preserve the transient peak current under a torque step:
    (λ_i, λ_e): (0.2, 0.5), (0.3, 0.6), (0.6, 0.6), (0.7, 0.7), (1, 0.7), (1, 0.9), (0.9, 1), (0.4, 1), (0.4, 0.7).
  - To improve or preserve the transient speed drop value under a torque step:
    (λ_i, λ_e): (0.1, 0.1), (1, 0.1), (1, 0.9), (0.9, 1), (0.1, 1)

7. Extension to Other Torque and Speed Changes

In this section, the previous pairing criteria are extended to other torque and speed steps, which involve more profound changes. Therefore, to illustrate the impact of the λ_e and λ_i pairing on the DC motor under different speed steps, in Figure 14, the influence of λ_e and λ_i is summarized across different metrics for the predefined speed step (from 95% to 100% of the rated speed, filled with color) and for a more pronounced speed step, i.e., a step from 90% to 100% of the rated speed (transparent with no colors).

It can be deduced from the graphs in Figure 14 that the rise time levels in the speed signal with the more profound speed step are quite similar compared to those observed under the predefined speed step. However, the overshoot in the speed signal is increased with low λ_e and high λ_i values, as the maximum overshoot level in the speed signal reaches 2.5%, in comparison to the 1% achieved with the predefined speed step. In any case, for high λ_e and λ_i values, the overshoot levels of the speed signal are quite similar among speed the steps, and lower than 0.5%.

As for the transient peak current and torque during the transient speed steps, low λ_e and λ_i values promote larger peak values, moving from almost two to four times the rated current, and from 13 to 30 times the rated torque when comparing the predefined speed step with the more pronounced speed step. In any case, for high λ_e and λ_i values, the transient peak current and torque values of the DC motor adopt similar values among the speed steps, although they are slightly larger with the more pronounced steps. A peak

current is presented that is around 0.5–0.75 times the rated current for the predefined speed step vs. 1–1.5 times the rated current for the more pronounced speed step. As for the transient peak torque, it is around 4–5 times the rated torque with the predefined speed step vs. 6–7 times the rated torque with the more pronounced speed step.

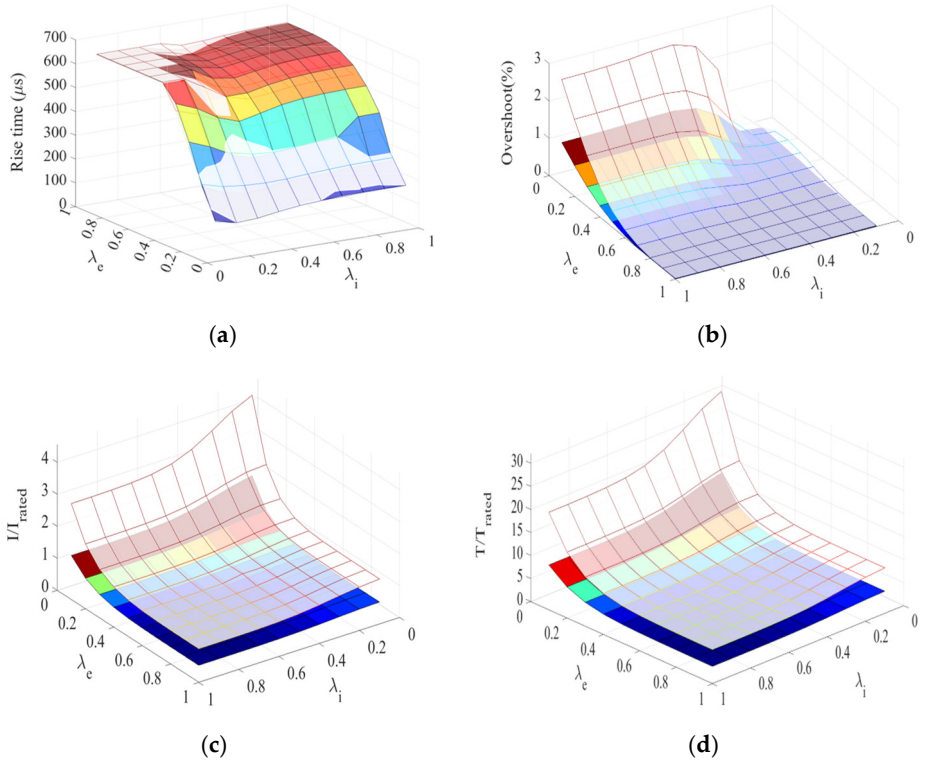

Figure 14. Pairing criteria of λ_e and λ_i for a FOCS-based DC motor subjected to the predefined speed step (from 95% to 100% rated speed, filled with colors) and different speed step (from 90% to 100% of rated speed), to allow for improvements in different criteria with respect to the IOCS-based DC motor: (**a**) rise time (μs) of speed signal, (**b**) overshoot (%) of speed signal, (**c**) peak current, and (**d**) peak torque. The areas in dark red represent similar or worse metric levels compared with the IOCS-based DC motor, while the areas in blue represent similar or better levels.

To illustrate the impact of the λ_e and λ_i pairing on the DC motor under different load torque steps, in Figure 15, the influence of λ_e and λ_i is summarized across different metrics for the predefined torque step (from 50% to 100% of the rated torque, filled with color) and for a more pronounced torque step, i.e., a step from 0% to 100% of the rated torque (transparent, with no colors). It can be deduced from the graphs in Figure 15 that the rise time levels in the torque signals are quite similar compared to those observed under the predefined torque step. However, the overshoot in the torque signal is increased for low λ_e and high λ_i values, as the maximum overshoot level in the torque signal reaches almost 30%, in comparison to the 10% achieved with the predefined torque step. In any case, for high λ_e and λ_i values, the overshoot level of the torque signal adopts similar values among the load torque steps, below 0.15%.

As for the transient peak current during the torque steps, low λ_e and high λ_i values promote a larger peak value, moving from almost 0.16 to 0.18 times the rated current when comparing the predefined with the more pronounced torque step. In any case, for high λ_e and λ_i values, the transient peak current values are quite similar among the torque steps, around 0.14 times the rated current. The transient speed drop during the more pronounced torque step lowers down to 0.98 times the rated speed, in comparison to 0.991 times with the predefined torque step.

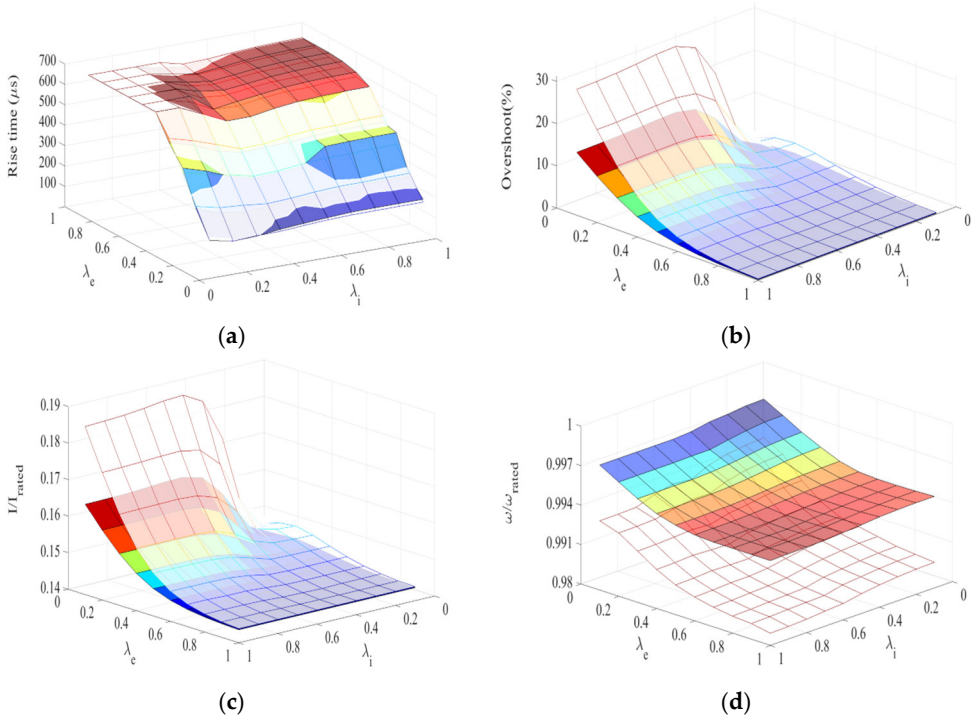

Figure 15. Pairing criteria of λ_e and λ_i for a FOCS-based DC motor subjected to the predefined torque step (from 50% to 100% rated torque, filled with colors) and a different torque step (from 0% to 100% of rated torque), to allow for improvements in different criteria with respect to the IOCS-based DC motor: (**a**) rise time (μs) of torque signal, (**b**) overshoot (%) of torque signal, (**c**) peak current, and (**d**) speed drop. The areas in dark red represent similar or worse metric levels compared with the IOCS-based DC motor, while the areas in blue represent similar or better levels.

In summary, for a wider range of speed and torque steps, low λ_e and λ_i values are not recommended, as they promote larger overshoot and transient peak current levels during both speed and torque steps. They are also not recommended as they foster greater transient peak torque during a speed step and a deeper speed drop during a torque step. Therefore, depending on the specific application in which the DC motor is used, certain peak current or torque values might be unacceptable. Similarly, exceeding specific overshoot limits in speed or torque signals, or experiencing a significant transient speed drop during a torque step, may also be restricted. Therefore, the previous analysis allows the reader to consider or discard certain λ_e and λ_i pairings according to a specific application and to impose specific saturations, or either adaptive or robust designs, to meet the specifications.

8. Conclusions

In the present paper, a thorough analysis for obtaining pairing criteria for λ_e and λ_i values for a FOCS-based DC motor under torque and speed steps was developed according to different metrics. For this purpose, Oustaloup's recursive approximation method was used to give a rational approximation of the fractional-order term, and such an approximation was implemented in the mathematical model of the FOCS-based DC motor. To deduce criteria for pairing the fractional exponents, λ_e and λ_i, a preliminary integer-order study was carried out to obtain the parameters for the integral and proportional current and speed loops within the IOCS-based DC motor and to set the base for the expected thresholds for the FOCS-based DC motor model. Based on this preliminary study, room for improvement in or preservation of the behavior of the IOCS-based DC motor were observed in different metrics, i.e., overshoot, rise time, peak current, peak torque during the speed step, and speed drop during the torque step, to be covered by the FOCS-based

DC motor. However, there is also room for a worsening of these metrics if the fractional exponents are not well combined. Therefore, a discussion was developed for obtaining proper pairing criteria for λ_e and λ_i to represent an improvement over the IOCS-based DC motor under torque and speed steps and different metrics, in both a separate and, finally, in a simultaneous way, by considering both robust and adaptive control design approaches. Furthermore, the criteria were extended to other speed and load torque changes that involve more profound steps, and conclusions about the shortcomings of certain pairings of fractional orders were pointed out.

Author Contributions: Conceptualization, M.H.-L.; methodology, M.H.-L.; software, M.H.-L. and A.G.-J.; validation, M.H.-L. and A.G.-J.; formal analysis, M.H.-L.; investigation, M.H.-L.; data curation, A.G.-J.; writing—original draft preparation, M.H.-L.; writing—review and editing, M.H.-L.; visualization, M.H.-L. and A.G.-J.; supervision, M.H.-L. All authors have read and agreed to the published version of the manuscript.

Funding: This research received no external funding.

Data Availability Statement: Data available on request due to privacy restrictions.

Conflicts of Interest: The authors declare no conflicts of interest.

References

1. Vu, T.N.L.; Chuong, V.L.; Truong, N.T.N.; Jung, J.H. Analytical Design of Fractional-Order PI Controller for Parallel Cascade Control Systems. *Appl. Sci.* **2022**, *12*, 2222. [CrossRef]
2. Vinagre, B.M.; Podlubny, I.; Hernandez, A.; Feliu, V. Some approximations of fractional order operators used in control theory and applications. *Fract. Calc. Appl. Anal.* **2000**, *3*, 231–248.
3. Yüce, A.; Deniz, F.N.; Tan, N. A New Integer Order Approximation Table for Fractional Order Derivative Operators. *IFAC-PapersOnLine* **2017**, *50*, 9736–9741. [CrossRef]
4. Mihaly, V.; Dulf, E. Novel Fractional Order Controller Design for First Order Systems with Time Delay. In Proceedings of the 2020 22nd IEEE International Conference on Automation, Quality and Testing, Robotics—THETA, AQTR 2020—Proceedings, Cluj-Napoca, Romania, 21–23 May 2020. [CrossRef]
5. Tepljakov, A.; Petlenkov, E.; Belikov, J.; Astapov, S. Digital Fractional-Order Control of a Position Servo | IEEE Conference Publication | IEEE Xplore. In Proceedings of the 20th International Conference Mixed Design of Integrated Circuits and Systems, Gdynia, Poland, 20–22 June 2013; pp. 462–467.
6. Tepljakov, A.; Petlenkov, E.; Belikov, J.; Gonzalez, E.A. Design of Retuning Fractional PID Controllers for a Closed-Loop Magnetic Levitation Control System. In Proceedings of the 2014 13th International Conference on Control Automation Robotics and Vision, ICARCV 2014, Singapore, 10–12 December 2014; pp. 1345–1350. [CrossRef]
7. Tepljakov, A.; Petlenkov, E.; Belikov, J.; Halas, M. Design and Implementation of Fractional-Order PID Controllers for a Fluid Tank System. In Proceedings of the American Control Conference, Washington, DC, USA, 17–19 June 2013; pp. 1777–1782. [CrossRef]
8. Heredero-Peris, D.; Sanchez-Sanchez, E.; Chillon-Anton, C.; Montesinos-Miracle, D.; Galceran-Arellano, S. A Novel Fractional Proportional-Resonant Current Controller for Voltage Source Converters. In Proceedings of the 2016 18th European Conference on Power Electronics and Applications, EPE 2016 ECCE Europe, Karlsruhe, Germany, 5–9 September 2016. [CrossRef]
9. Haro-Larrode, M.; Bergna-Diaz, G.; Eguia, P.; Santos-Mugica, M. On the Tuning of Fractional Order Resonant Controllers for a Voltage Source Converter in a Weak AC Grid Context. *IEEE Access* **2021**, *9*, 52741–52758. [CrossRef]
10. Lino, P.; Maione, G. Cascade Fractional-Order PI Control of a Linear Positioning System. *IFAC-PapersOnLine* **2018**, *51*, 557–562. [CrossRef]
11. Maione, G. Continued Fractions Approximation of the Impulse Response of Fractional-Order Dynamic Systems. *IET Control. Theory Appl.* **2008**, *2*, 564–572. [CrossRef]
12. Idir, A.; Canale, L.; Bensafia, Y.; Khettab, K. Design and Robust Performance Analysis of Low-Order Approximation of Fractional PID Controller Based on an IABC Algorithm for an Automatic Voltage Regulator System. *Energies* **2022**, *15*, 8973. [CrossRef]
13. Chuong, V.L.; Nam, N.H.; Giang, L.H.; Vu, T.N.L. Robust Fractional-Order PI/PD Controllers for a Cascade Control Structure of Servo Systems. *Fractal Fract.* **2024**, *8*, 244. [CrossRef]

14. Vavilala, S.K.; Thirumavalavan, V.; Chandrasekaran, K. Level Control of a Conical Tank Using the Fractional Order Controller. *Comput. Electr. Eng.* **2020**, *87*, 106690. [CrossRef]
15. Frikh, M.L.; Soltani, F.; Bensiali, N.; Boutasseta, N.; Fergani, N. Fractional Order PID Controller Design for Wind Turbine Systems Using Analytical and Computational Tuning Approaches. *Comput. Electr. Eng.* **2021**, *95*, 107410. [CrossRef]
16. Frikh, M.L.; Boutasseta, N. Pitch Angle Control of Wind Turbines Using Model-Free Auto-Tuned Fractional Order Proportional Derivative ATFOPD Controller. *Comput. Electr. Eng.* **2024**, *116*, 109199. [CrossRef]
17. Tepljakov, A.; Vunder, V.; Petlenkov, E.; Nakshatharan, S.S.; Punning, A.; Kaparin, V.; Belikov, J.; Aabloo, A. Fractional-Order Modeling and Control of Ionic Polymer-Metal Composite Actuator. *Smart Mater. Struct.* **2019**, *28*, 084008. [CrossRef]
18. Chao, H.; Luo, Y.; Di, L.; Chen, Y.Q. Roll-Channel Fractional Order Controller Design for a Small Fixed-Wing Unmanned Aerial Vehicle. *Control. Eng. Pract.* **2010**, *18*, 761–772. [CrossRef]
19. Guan, H.; Sun, X.; Su, Y.; Hu, T.; Wang, H.; Wang, H.; Peng, C.; Guo, Q. UAV-Lidar Aids Automatic Intelligent Powerline Inspection. *Int. J. Electr. Power Energy Syst.* **2021**, *130*, 106987. [CrossRef]
20. Larrauri, J.I.; Sorrosal, G.; Gonzalez, M. Automatic System for Overhead Power Line Inspection Using an Unmanned Aerial Vehicle—RELIFO Project. In Proceedings of the 2013 International Conference on Unmanned Aircraft Systems, ICUAS 2013—Conference Proceedings, Atlanta, GA, USA, 28–31 May 2013; pp. 244–252. [CrossRef]
21. Alhassan, A.B.; Zhang, X.; Shen, H.; Xu, H. Power Transmission Line Inspection Robots: A Review, Trends and Challenges for Future Research. *Int. J. Electr. Power Energy Syst.* **2020**, *118*, 105862. [CrossRef]
22. Elizondo, D.; Gentile, T.; Candia, H.; Bell, G. Overview of Robotic Applications for Energized Transmission Line Work—Technologies, Field Projects and Future Developments. In Proceedings of the 2010 1st International Conference on Applied Robotics for the Power Industry, CARPI 2010, Montreal, QC, Canada, 5–7 October 2010. [CrossRef]
23. Sudhakar, S.; Vijayakumar, V.; Sathiya Kumar, C.; Priya, V.; Ravi, L.; Subramaniyaswamy, V. Unmanned Aerial Vehicle (UAV) Based Forest Fire Detection and Monitoring for Reducing False Alarms in Forest-Fires. *Comput. Commun.* **2020**, *149*, 1–16. [CrossRef]
24. Rathod, T.; Patil, V.; Harikrishnan, R.; Shahane, P. Multipurpose Deep Learning-Powered UAV for Forest Fire Prevention and Emergency Response. *HardwareX* **2023**, *16*, e00479. [CrossRef]
25. Lee, S.Y.; Han, S.R.; Song, B.D. Simultaneous Cooperation of Refrigerated Ground Vehicle (RGV) and Unmanned Aerial Vehicle (UAV) for Rapid Delivery with Perishable Food. *Appl. Math. Model.* **2022**, *106*, 844–866. [CrossRef]
26. He, X.; Tao, M.; Xie, S.; Chen, Q. Neuro-Adaptive Singularity-Free Finite-Time Attitude Tracking Control of Quadrotor UAVs. *Comput. Electr. Eng.* **2021**, *96*, 107485. [CrossRef]
27. García, R.A.; Rubio, F.R.; Ortega, M.G. Robust PID Control of the Quadrotor Helicopter. *IFAC Proc. Vol.* **2012**, *45*, 229–234. [CrossRef]
28. Hoffmann, G.M.; Huang, H.; Waslander, S.L.; Tomlin, C.J. Quadrotor Helicopter Flight Dynamics and Control: Theory and Experiment. *Collect. Tech. Pap.—AIAA Guid. Navig. Control. Conf.* **2007**, *2*, 1670–1689. [CrossRef]
29. Ding, L.; Wang, Z. A Robust Control for an Aerial Robot Quadrotor under Wind Gusts. *J. Robot.* **2018**, *2018*, 5607362. [CrossRef]
30. Guedida, S.; Tabbache, B.; Benzaoui, K.M.S.; Nounou, K.; Nesri, M. Novel Speed Sensorless DTC Design for a Five-Phase Induction Motor with an Intelligent Fractional Order Controller Based-MRAS Estimator. *Power Electron. Drives* **2024**, *9*, 63–85. [CrossRef]
31. Barrero, F.; Satué, M.G.; Colodro, F.; Arahal, M.R. Tuning of Modern Speed Drives Using IFOC: A Case Study for a Five-Phase Induction Machine. *Results Eng.* **2024**, *24*, 103145. [CrossRef]
32. Kumarasamy, V.; KarumanchettyThottam Ramasamy, V.; Chandrasekaran, G.; Chinnaraj, G.; Sivalingam, P.; Kumar, N.S. A Review of Integer Order PID and Fractional Order PID Controllers Using Optimization Techniques for Speed Control of Brushless DC Motor Drive. *Int. J. Syst. Assur. Eng. Manag.* **2023**, *14*, 1139–1150. [CrossRef]
33. Burridge, M.J.; Qu, Z. An Improved Nonlinear Control Design for Series DC Motors. *Comput. Electr. Eng.* **2003**, *29*, 273–288. [CrossRef]
34. Yildiz, A.B. Electrical Equivalent Circuit Based Modeling and Analysis of Direct Current Motors. *Int. J. Electr. Power Energy Syst.* **2012**, *43*, 1043–1047. [CrossRef]
35. Singhal, R.; Padhee, S.; Kaur, G. Design of Fractional Order PID Controller for Speed Control of DC Motor. *Int. J. Sci. Res. Publ.* **2012**, *2*.
36. Tzounas, G.; Dassios, I.; Murad, M.A.A.; Milano, F. Theory and Implementation of Fractional Order Controllers for Power System Applications. *IEEE Trans. Power Syst.* **2020**, *35*, 4622–4631. [CrossRef]
37. Tepljakov, A. FOMCON Toolbox for MATLAB—File Exchange—MATLAB Central. Available online: https://es.mathworks.com/matlabcentral/fileexchange/66323-fomcon-toolbox-for-matlab (accessed on 2 July 2024).

38. Yüce, A.; Tan, N.; Atherton, D.P. Fractional Order PI Controller Design for Time Delay Systems. *IFAC-PapersOnLine* **2016**, *49*, 94–99. [CrossRef]
39. Arahal, M.R.; Satué, M.G.; Colodro, F.; Martínez-Heredia, J.M. Trade-Off Analysis of Drive Dynamics Considering Speed and Current Loops. *Energies* **2024**, *17*, 3649. [CrossRef]